Inorganic Chemistry

Article

pubs.acs.org/IC

Subcomponent Self-Assembly of Rare-Earth Single-Molecule Magnets

Victoria E. Campbell,*[,†] Régis Guillot,[†] Eric Riviere,[†] Pierre-Thomas Brun,[‡] Wolfgang Wernsdorfer,[§] and Talal Mallah[†]

[†]Institut de Chimie Moléculaire et des Matériaux d'Orsay, CNRS, Université de Paris Sud 11, 91405 Orsay Cedex, France

[‡]LFMI, École Polytechnique Fédérale de Lausanne, 1015 Lausanne, Switzerland

[§]Institut Néel, CNRS, Université J. Fourier, BP 166 25, Avenue des Martyrs, 38405 Grenoble, France

Supporting Information

ABSTRACT: A family of lanthanide complexes has been synthesized by the subcomponent self-assembly methodology. Molecular architectures, which were stable in solution and under ambient conditions, were designed by the in situ formation of ligands around lanthanide ion templates. Magnetic studies indicated that, despite the low C_2 symmetry, **1** and **2** display single molecule magnet (SMM) behavior, with **1** exhibiting an effective energy barrier of the relaxation of the magnetization U_{eff}/k_B = 50 K and the pre-exponential factor $\tau_o = 6.80 \times 10^{-7}$ s. Step-like features in the hysteresis loops indicate the presence of quantum tunneling of the magnetization (QTM).

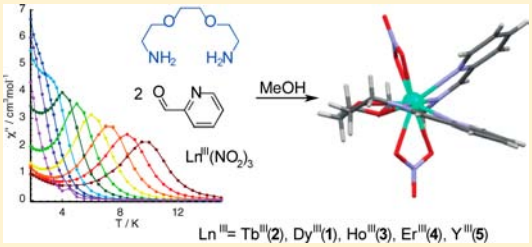

INTRODUCTION

In nature, order and functionality are often created though the self-assembly of multiple, chemically distinct building blocks. In recent years, self-assembly and more particularly subcomponent self-assembly have emerged as a powerful tool in the construction of elegant and intricate molecules.[1] With this last approach a variety of molecular architectures and systems have been designed *via* the in situ formation of ligands around metal ion templates starting from small building blocks.[2] Traditionally templated synthesis has been carried out around transition metal ions, which have a predictable coordination sphere and geometry.[3] In contrast, lanthanide ions, with their variable coordination numbers (CN = 6−12) and geometries have not been exploited so far as templates in supramolecular chemistry. In recent years, lanthanide ions have been the focus of considerable research, particularly for their optical[4] and magnetic properties.[5] Lanthanide coordination complexes have gained significant attention in the field of molecular magnetism, as they may behave as single-molecule magnets (SMM) due to their large magnetic anisotropy.[1d,6] At the molecular level, these bistable molecules exhibit slow magnetic relaxation at low temperatures and display magnetic hysteresis.[7] Such molecules offer the possibility to create quantum information devices that use spins to manipulate or store information.[8]

In the quest for discovering new SMM molecules, remarkable results have been obtained with lanthanide mononuclear complexes. For example Ishikawa and co-workers reported very large energy barriers for the relaxation of the magnetization of phthalocyanine (Pc) double-decker complexes of terbium(III) and dysprosium(III).[6a] Similar behavior was reported for an erbium(III) ion sandwiched between polyoxometallate ligands.[9] Among the lanthanides, the largest number of monolanthanide SMMs contains Dy^{III} ions.[10] This phenomenon can be explained by the reduced predisposition in Dy^{III} systems to show quantum tunneling of the magnetization (QTM) as well as by the high moment and high anisotropy of the Dy^{III} ion, which has a Kramer ground state ($S = 5/2$, $L = 5$, $^6H_{15/2}$, $g = 4/3$). The synthetic strategy employed thus far for monolanthanide SMMs has relied on the synthesis of polydentate ligands followed by lanthanide-ion complexation. For example, Sessoli and co-workers reported that a Dy/DOTA complex shows SMM behavior with an effective energy barrier of ca. 60 K.[10a]

Herein, we demonstrate that subcomponent self-assembly may be employed in the construction of Ln^{III}-containing edifices where the lanthanide ion is employed as a template. With this synthetic approach we are able to use commercially available simple building blocks toward the construction, in one step, of relatively complex architectures in which the ligand and complex are simultaneously formed. Thus, synthesizing assemblies are stable in solution, under ambient conditions, and display SMM behavior.

EXPERIMENTAL SECTION

General. All reactions were carried out in a 20 mL scillation vial. Unless otherwise stated, all reagents were purchased from Aldrich or TCI and used without further purification. MeOH was dried by distillation over calcium hydride.

Synthesis of Dy^{III}–N,N′-bis-pyridin-2-yl-methelene-1,8-diamino-3,6-dioxaoctane: Complex 1. To a 20 mL scillation vial, 2-

Received: January 14, 2013
Published: April 19, 2013

   dx.doi.org/10.1021/ic400098c | Inorg. Chem. 2013, 52, 5194−5200

formyl pyridine (43.3 μL, 4.46 × 10^{-4} mol), 1,8-diamino-3,6-dioxaoctane (32.2 μL, 2.23 × 10^{-4} mol), and 5 mL of dry MeOH were added and stirred at 323 K for 5 min. To this solution, a solution $Dy(NO_3)_3 5H_2O$ (0.1 g, 2.23 × 10^{-4} mol) in 1 mL of dry MeOH was added dropwise and left at 323 K for 3 h. The product was purified by vapor diffusion of Et_2O into the methanol solution of **1** (m = 0.112 g, yield = 80%). IR (ν/cm^{-1}): 3077.47, 2948.17, 2888.71, 2524.47, 2162.88, 1980.39, 1779.93, 1741.07, 1665.43, 1625.92, 1598.81, 1571.27, 1469.16, 1445.36, 1366.04, 1351.59, 1289.21, 1225.42, 1156.48, 1103.43, 1090.13, 1050.64, 1033.51, 1010.07, 987.86, 962.66, 935.47, 895.48, 871.63, 813.19, 784.18, 742.61, 704.82, 662.63, 634.58. ESI-MS: m/z 284.13 ($[\mathbf{1}(-NO_3)(MeOH)]^{2+}$; $[(\mathbf{1})_2(H_2O)_3]^{2+}$). Elem Anal. Calcd for $C_{19}H_{30}N_9O_{20}Dy$: C, 26.32; H. 3.49; N, 14.54. Found: C, 26.25; H, 2.65; N, 13.81.

Synthesis of Tb^{III}–N,N′-bis-pyridin-2-yl-methelene-1,8-diamino-3,6-dioxaoctane: Complex 2. To a 20 mL scillation vial, 2-formyl pyridine (44.7 μL, 4.59 × 10^{-4} mol), 1,8-diamino-3,6-dioxaoctane (33.6 μL, 2.29 × 10^{-4} mol), and 5 mL of dry MeOH were added and stirred at 323 K for 5 min. To this solution, a solution of $Tb(NO_3)_3 5H_2O$ (0.1 g, 2.29 × 10^{-4} mol) in 1 mL of dry MeOH was added dropwise and left at 323 K for 3 h. The product was purified by vapor diffusion of Et_2O into the methanol solution of **2** (m = 0.0917 g, yield = 65%). IR (ν/cm^{-1}): 3075.08, 2946.23, 2888.39, 2524.41, 2161.95, 2009.96, 1778.66, 1740.19, 1664.90, 1625.01, 1598.34, 1570.63, 1467.83, 1444.89, 1365.80, 1351.41, 1287.37, 1225.04, 1156.02, 1123.35, 1103.27, 1089.70, 1050.21, 1032.27, 1009.79, 987.64, 962.06, 946.39, 935.17, 895.34, 871.26, 813.39, 783.43, 741.96, 703.77, 662.36, 634.38. ESI-MS: m/z 609.7 ($[\mathbf{2}]^{1+}$). Elem Anal. Calcd for $C_{18}H_{28}N_9O_{20}Tb$: C, 25.45; H, 3.32; N, 14.48. Found: C, 25.74; H, 2.61; N, 13.59.

Synthesis of Ho^{III}–N,N′-bis-pyridin-2-yl-methelene-1,8-diamino-3,6-dioxaoctane: Complex 3. To a 20 mL scillation vial, 2-formyl pyridine (43.1 μL, 4.46 × 10^{-4} mol), 1,8-diamino-3,6-dioxaoctane (32.4 μL, 2.26 × 10^{-4} mol), and 5 mL of dry MeOH were added and stirred at 323 K for 5 min. To this solution, a solution of $Ho(NO_3)_3 5H_2O$ (0.1 g, 2.26 × 10^{-4} mol) in 1 mL of dry MeOH was added dropwise and left at 323 K for 3 h. The product was purified by vapor diffusion of Et_2O into the methanol solution of **3** (m = 0.0799 g, yield = 56%). IR (ν/cm^{-1}): 3077.46, 2944.29, 2887.22, 2524.45, 2164.02, 2002.86, 1778.95, 1740.86, 1665.25, 1625.45, 1598.72, 1570.99, 1468.23, 1445.09, 1365.96, 1351.44, 1288.53, 1225.50, 1156.36, 1103.37, 1090.17, 1050.35, 1033.59, 1010.19, 987.76, 962.06, 935.67, 895.43, 871.83, 813.29, 783.84, 742.89, 703.97, 662.63, 634.48. ESI-MS: m/z 266.13 ($[\mathbf{3}(-NO_3)]^{2+}$). Elem Anal. Calcd for $C_{19}H_{42}N_8O_{23}Ho$: C, 24.93; H, 4.62; N, 12.24. Found: C, 24.55; H, 3.58; N, 12.44.

Synthesis of Er^{III}–N,N′-bis-pyridin-2-yl-methelene-1,8-diamino-3,6-dioxaoctane: Complex 4. To a 20 mL scillation vial, 2-formyl pyridine (53.8 μL, 5.66 × 10^{-4} mol), 1,8-diamino-3,6-dioxaoctane (40.5 μL, 2.83 × 10^{-4} mol), and 5 mL of dry MeOH were added and stirred at 323 K for 5 min. To this solution, a solution of $Er(NO_3)_3H_2O$ (0.1 g, 2.83 × 10^{-4} mol) in 1 mL of dry MeOH was added dropwise and left at 323 K for 3 h. The product was purified by vapor diffusion of Et_2O into the methanol solution of **4** (m = 0.0853 g, yield = 48%). IR (ν/cm^{-1}): 3076.55, 2945.65, 2880.25, 2524.74, 2163.04, 2001.86, 1782.96, 1739.13, 1663.25, 1625.56, 1597.82, 1570.21, 1468.40, 1445.69, 1365.88, 1351.37, 1289.63, 1225.91, 1156.08, 1103.39, 1087.95, 1050.63, 1032.69, 1010.87, 987.13, 962.46, 935.88, 895.63, 871.41, 813.36, 782.99, 743.09, 704.07, 662.81, 634.04. ESI-MS: m/z 651.28 ($[\mathbf{4}(MeOH)]^{1+}$). Elem Anal. Calcd for $C_{19}H_{26}N_7O_{12}Er$: C, 32.06; H, 3.68; N, 13.78. Found: C, 30.31; H, 3.64; N, 13.83.

Synthesis of Y^{III}–N,N′-bis-pyridin-2-yl-methelene-1,8-diamino-3,6-dioxaoctane: Complex 5. To a NMR tube, 2-formyl pyridine (4.9 μL, 5.22 × 10^{-5} mol), 1,8-diamino-3,6-dioxaoctane (3.7 μL, 2.61 × 10^{-5} mol), and 0.5 mL of dry MeOD-d_4 were added and stirred at 323 K for 5 min. To this solution, a solution of $Y(NO_3)_3H_2O$ (0.01 g, 2.61 × 10^{-5} mol) in 0.1 mL of dry MeOD-d_4 was added dropwise and left at 323 K for 3 h. ^{1}H NMR (300 MHz, 300 K, MeOD-d_4): δ 8.65 (d, 2H), 7.92–786 (m, 4H), 7.46 (t, 2H), 3.72 (t, 8H), 3.52 (s, 4H). ^{1}H NMR (300 MHz, 300 K, DMSO-d_6): δ 8.63 (d, 2H), 8.32 (s, 1H), 7.92–786 (m, 4H), 7.46 (t, 2H), 3.73 (t, 8H), 3.53 (s, 4H). ^{1}NMR was taken after one week; no changes in the chemical shifts were observed. IR (ν/cm^{-1}): 3076.08, 2945.62, 2889.02, 2521.75, 2163.05, 1999.86, 1782.61, 1739.13, 1663.04, 1623.71, 1597.82, 1572.99, 1467.39, 1445.65, 1358.96, 1290.49, 1225.46, 1156.82, 1103.73, 1090.31, 1050.57, 1033.18, 1010.09, 987.03, 962.55, 935.28, 895.49, 871.64, 813.68, 784.04, 741.46, 704.01, 662.67, 634.88. ESI-MS: m/z 539.05 ($[\mathbf{5}]^{1+}$). Elem Anal. Calcd for $C_{39}H_{56}N_{17}O_{34}Y$: C, 29.77; H, 3.59; N, 15.13. Found: C, 29.40; H, 3.50; N, 15.61.

EA, IR, ESI-MS, and NMR Spectroscopy. ESI-MS spectra were recorded on a Thermo Scientific 2009 mass spectrometer. NMR spectra were recorded on a Bruker Aspect 300 NMR spectrometer. IR spectra were recorded on a Bruker TENSOR-27 FT-IR spectrometer equipped with an attenuated total reflectance (ATR) sample holder in the 4000–500 cm^{-1} range.

Single Crystal X-Ray Diffraction Studies. X-ray diffraction data were collected by using a Kappa X8 APPEX II Bruker diffractometer with graphite-monochromated Mo Kα radiation (λ = 0.71073 Å). Crystals were mounted on a CryoLoop (Hampton Research) with Paratone-N (Hampton Research) as a cryoprotectant and then flash-frozen in a nitrogen-gas stream at 100 K. The temperature of the crystal was maintained at the selected value (100K) by means of a 700 series Cryostream cooling device to within an accuracy of ±1 K. The data were corrected for Lorentz polarization and absorption effects. The structures were solved by direct methods using SHELXS-97[11] and refined against F^2 by full-matrix least-squares techniques using SHELXL-97[12] with anisotropic displacement parameters for all non-hydrogen atoms. Hydrogen atoms were located on a difference Fourier map and introduced into the calculations as a riding model with isotropic thermal parameters. All calculations were performed using the Crystal Structure crystallographic software package WINGX.[13]

Magnetic Measurements. The magnetic susceptibility measurements were obtained using a Quantum Design SQUID magnetometer MPMS-XL7 operating between 1.8 and 300 K for DC-applied fields ranging from −7 to 7 T. DC analysis was performed on polycrystalline samples of **1** and **2** (17.61 mg and 17.31 mg, respectively) wrapped in eicosan under a field between 0.1 and 1 T and between 1.8 and 300 K. AC susceptibility measurements were carried out under an oscillating field of 1.5 or 3 Oe and AC frequencies ranging between 0.1 and 1500 Hz. Diamagnetic corrections were applied for the sample holder and the eicosan.

Micro-SQUID Measurements. Magnetization measurements on oriented single crystals were carried out with an array of micro-SQUIDs.[14] This magnetometer works in the temperature range of 0.04 to 7 K and in fields of up to 0.8 T with sweeping rates as high as 0.28 Ts^{-1} and exhibits field stability of better than mT. The time resolution is approximately 1 ms. The field can be applied in any direction of the micro-SQUID plane with precision greater than 0.1° by separately driving three orthogonal coils. In order to ensure good thermalization, a single crystal was fixed with apiezon grease.

RESULTS AND DISCUSSION

Synthesis. The one pot reaction between 2-formyl pyridine (2 equiv.) and 1,8-diamino-3,6-dioxaoctane with the corresponding hydrated $Ln(NO_3)_3$ salt (1 equiv.) in MeOH afforded bisimine complexes in yields ranging from 50 to 80% (Scheme 1). The complexes were purified by recrystallization from diethyl ether affording off-white X-ray quality crystals. FT-IR spectra are superimposable for all complexes and indicate that no residual aldehyde is left (Figures S22–26 Supporting Information), as the characteristic band for the C=O stretch is not present at 1725–1715 cm^{-1}. Further confirmation of imine formation is given by the C=N band present in all compounds at 1625 cm^{-1}. In order to probe into the complex stability in solution, ESI-MS was performed on all samples, and ^{1}H NMR was performed on **5**, as Y^{III}, which is diamagnetic, has a

dx.doi.org/10.1021/ic400098c | Inorg. Chem. 2013, 52, 5194–5200

Scheme 1. Subcomponent Self-Assembly of a Family of Lanthanide-Ion Complexes

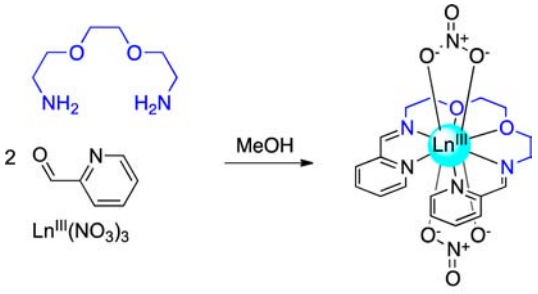

Ln^{III} = Tb^{III} (**2**), Dy^{III} (**1**), Ho^{III} (**3**), Er^{III} (**4**), Y^{III} (**5**)

comparable ionic radius to Dy^{III}. Therefore, it is possible to replace Y^{III} for Dy^{III} to gain insight into the solution dynamics of these self-assembled complexes. Complex **5** was stable in solution over a period of several weeks and at varying concentrations.

Crystal Structures. Single crystal X-ray analysis of **1**−**5** revealed that the complexes have low C_2 symmetry, which is in contrast to what is found for the majority of monolanthanide SMMs that are found with a high-order local symmetry.[6a,10a,c] As noted in Table 1, complexes **1** (Figure 1), **3** (Figure S2), and **4** (Figure S3) were isostructural and crystallized in the triclinic $P\bar{1}$ space group, while **2** (Figure S1) and **5** (Figure S4) crystallized in the monoclinic $P2_1/n$ and $P2_1/c$ space groups, respectively. Although the complexes crystallize in different space groups, the arrangement of the ligand around the lanthanide ion remains unchanged; therefore only the dysprosium complex (**1**) will be described in more detail. Bond distances for all compounds are reported in Table 2. The

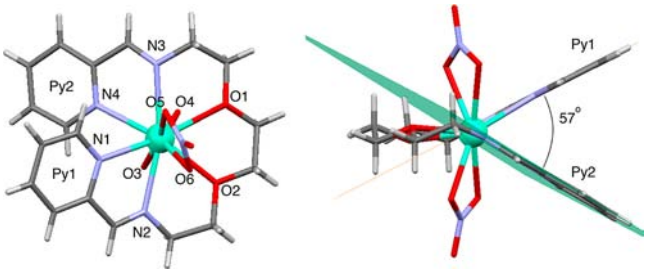

Figure 1. X-ray crystal structure of complex **1**: C = gray, O = red, N = lilac, H = white, and Dy = teal. Solvent molecule and counterions are omitted for clarity.

Dy^{III} ion is coordinated between four nitrogen atoms and six oxygen atoms with Dy−N bonds of 2.483−2.585 Å and Dy−O bonds of 2.430−2.493 Å; four of the oxygen atoms come from the coordinated nitrate ions. Two oxygen (O1 and O1) and two nitrogen (N2 and N3) atoms are arranged on an equatorial plane around the Dy^{III} ion. Due to steric bulk of the pyridine rings (Py1 and Py2), N1 and N2 are twisted out of this mean plane. The dihedral angle between the planes formed by Py1 and Py2 is 57° for **1** (Figure 1) and is comparable for the other complexes (see the Supporting Information). In this system, the lanthanide ion acts as a template around which the ligand is organized. The analysis of the packing arrangement reveals that there are no strong intermolecular forces between neighboring molecules (Figure 2). There is one molecule of methanol in the crystal lattice, and the charge balance is given by one nitrate counterion.

The lanthanide inner coordination sphere is far from an idealized geometry and may best be described as a distorted bicapped square antiprism (Figure 3). Two trapezes may be

Table 1. Crystallographic Data for the Series of Self-Assembled Lanthanide-Ion Complexes

compound	**1**	**2**	**3**	**4**	**5**
formula	$C_{19}H_{26}DyN_7O_{12}$	$C_{19}H_{26}TbN_7O_{12}$	$C_{19}H_{26}HoN_7O_{12}$	$C_{19}H_{26}ErN_7O_{12}$	$C_{39}H_{56}Y_3N_{17}O_{34}$
fw	706.97	703.40	709.40	711.73	1573.74
cryst size/mm^3	0.19 × 0.12 × 0.04	0.31 × 0.17 × 0.04	0.21 × 0.17 × 0.03	0.31 × 0.09 × 0.07	0.21 × 0.06 × 0.02
cryst syst	triclinic	monoclinic	triclinic	triclinic	monoclinic
space group	$P\bar{1}$	$P2_1/n$	$P\bar{1}$	$P\bar{1}$	$P2_1/c$
a, Å	7.893(4)	15.9678(4)	7.898(5)	7.9429(5)	8.0457(9)
b, Å	11.861(5)	8.0138(2)	11.870(5)	11.9438(6)	23.211(3)
c, Å	13.990(5)	21.4325(5)	13.941(5)	13.857(8)	32.381(4)
α, deg	92.479(5)	90	92.454(5)	91.998(10)	90.00
β, deg	95.807(5)	109.7500(10)	95.762(5)	95.893(2)	94.444(6)
γ, deg	94.319(5)	90	94.560(5)	94.797(10)	90.00
cell volume, Å^3	1297.6(11)	2581.23(11)	1294.5(11)	1301.81(13)	6028.9(12)
Z	2	4	2	2	4
T, K	100(1)	100(1)	100(1)	100(1)	100(1)
F_{000}	702	1400	704	706	3192
μ/mm^{-1}	2.953	2.814	3.130	3.297	2.974
θ range/deg	1.72−30.69	1.39−30.62	1.72−33.13	2.32−30.56	1.08−26.48
reflns collected	31 722	58 440	32 315	40 698	72 250
reflns unique	7 653	7 770	8 896	10 872	11 037
R_{int}	0.0314	0.0191	0.0262	0.0240	0.1214
GOF	1.098	1.154	1.167	1.072	1.005
reflns obsd. ($I > 2\sigma(I)$)	6 970	7 051	7 741	9 500	4763
params	354	354	354	354	836
wR_2 (all data)	0.1089	0.0565	0.1122	0.0736	0.2380
R value ($I > 2\sigma(I)$)	0.0385	0.0232	0.0459	0.0296	0.0844
largest diff. peak and hole (e·Å^{-3})	−1.775; 1.861	−0.897; 1.836	−2.571; 2.683	−1.978; 3.038	−1.634; 0.881

dx.doi.org/10.1021/ic400098c | Inorg. Chem. 2013, 52, 5194−5200

Table 2. Selected Bond Distances

1		2		3		4		5	
Dy–N1	2.585(3) Å	Tb–N1	2.6092(19) Å	Ho–N1	2.574(4) Å	Er–N1	2.570(2) Å	Y–N1	2.571(8) Å
Dy–N2	2.483(4) Å	Tb–N2	2.5072(19) Å	Ho–N2	2.473(4) Å	Er–N2	2.463(2) Å	Y–N2	2.484(10) Å
Dy–N3	2.503(3) Å	Tb–N3	2.5203(19) Å	Ho–N3	2.495(4) Å	Er–N3	2.485(2) Å	Y–N3	2.473(9 Å)
Dy–N4	2.552(3) Å	Tb–N4	2.5761(19) Å	Ho–N4	2.540(4) Å	Er–N4	2.5366(19) Å	Y–N4	2.557(9) Å
Dy–O1	2.493(3) Å	Tb–O1	2.5124(17) Å	Ho–O1	2.462(3) Å	Er–O1	2.4706(19) Å	Y–O1	2.459(7) Å
Dy–O2	2.478(3) Å	Tb–O2	2.5259(17) Å	Ho–O2	2.482(4) Å	Er–O2	2.4572(18) Å	Y–O2	2.465(7) Å
Dy–O3	2.540(3) Å	Tb–O3	2.4757(17) Å	Ho–O3	2.477(4) Å	Er–O3	2.5380(18) Å	Y–O3	2.422(7) Å
Dy–O4	2.455(3) Å	Tb–O4	2.5194(18) Å	Ho–O4	2.419(4) Å	Er–O4	2.4382(18) Å	Y–O4	2.488(7) Å
Dy–O5	2.490(3) Å	Tb–O5	2.4310(16) Å	Ho–O5	2.446(3) Å	Er–O5	2.4766(18) Å	Y–O5	2.447(7) Å
Dy–O6	2.430(3) Å	Tb–O6	2.4980(17) Å	Ho–O6	2.536(4) Å	Er–O6	2.4177(19) Å	Y–O6	2.520(7) Å

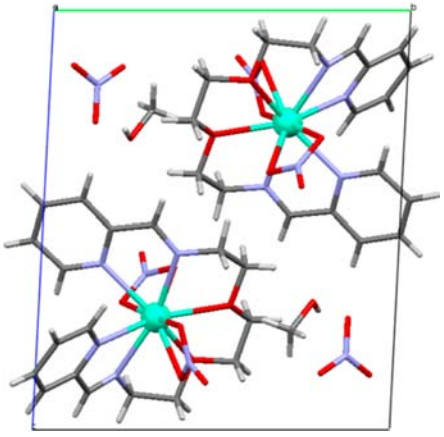

Figure 2. View along *a* axis of the crystal packing of complex **1**: C = gray, O = red, N = lilac, H = white, and Dy = teal.

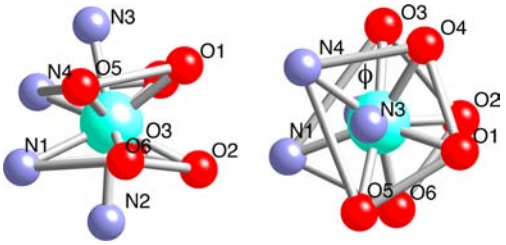

Figure 3. Perspective showing the distorted bicapped square-antiprismatic coordination geometry of the central Dy^{III} ion of **1**.

defined by the mean planes through four of the coordinating atoms (O1, O4, N4, O5 and O3, O2, N1, O6). The first deviation from an idealized geometry is immediately noticeable, as the atoms do not form a square but a trapeze. The two trapezes are twisted at a skew angle of $\phi = 58°$ with respect to one another (Figure 3). This angle is far from the expected value for an ideal D_{4d} symmetry ($\phi = 45°$). The second deviation arises from the dihedral angle between the two mean planes, which are at 10° with respect to one another. In an ideal D_{4d} symmetry, the two mean planes are parallel. Therefore, the coordination geometry may be best described as a very distorted bicapped square antiprism.

CCDC 911884, 911886, 911885, 925512, and 925513 contain the supplementary crystallographic data for this paper. These data can be obtained free of charge from the Cambridge Crystallographic Data Centre via www.ccdc.cam.ac.uk/data_request/cif.

Magnetic Properties. DC magnetic susceptibility measurements were carried out between 2 and 300 K at 1000 and 10 000 Oe (Figures 4 and S09). At room temperature, $\chi_M T$ = 13.71, 11.43, 13.25, and 11.65 for complexes **1**–**4**, respectively,

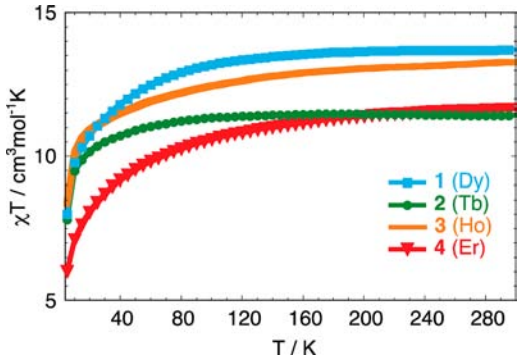

Figure 4. Temperature dependence of the χT product at 10 000 Oe for complexes **1**–**4**.

which are in good agreement with the expected values for mononuclear Dy^{III} ($S = 5/2$, $L = 5$, $^6H_{15/2}$, $g = 4/3$, $\chi_M T_{\text{free ion}}$ = 14.17), Tb^{III} ($S = 3$, $L = 3$, $^7F_6$, $g = 3/2$, $\chi_M T_{\text{free ion}}$ = 11.81), Ho^{III} ($S = 2$, $L = 6$, $^5I_8$, $g = 5/4$, $\chi_M T_{\text{free ion}}$ = 14.48), and Er^{III} ($S = 3/2$, $L = 6$, $^4I_{15/2}$, $g = 36/5$, $\chi_M T_{\text{free ion}}$ = 11.48) complexes. Due to the thermal depopulation of the Stark sublevels and to the presence of significant anisotropy, the $\chi_M T$ values decrease at low temperatures.

The magnetization (M) vs field (H) plots display field dependence of the magnetization, which does not saturate at high fields (up to 1 T) and at low temperatures (2 K; Figures 5 and S05–S08). This behavior is indicative of highly magnetically anisotropic systems.

Dynamic susceptibility measurements were carried out on complexes **1**–**4**. Of the series, only **1** (Dy) and **2** (Tb)

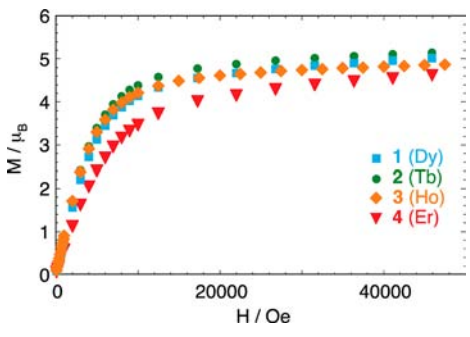

Figure 5. Field dependence of the magnetization at 2 K for complexes **1**–**4**.

dx.doi.org/10.1021/ic400098c | Inorg. Chem. 2013, 52, 5194–5200

displayed frequency dependence of the out-of-phase magnetic susceptibility (χ''). In order to investigate the potential SMM behavior of **1** and **2**, AC magnetic susceptibility measurements were carried out under zero DC field. The frequency dependence of χ'', which is symptomatic of slow relaxation and SMM behavior, indicated that these complexes undergo a slow relaxation of the magnetization below 10 K (Figure S11). However, no maxima for χ'' were seen in the temperature and frequency range studied. This behavior may be attributed to small energy barriers resulting from quantum tunneling of magnetizations (QTM), which is commonly reported for lanthanide-containing complexes. QTM occurs when under an appropriate magnetic field, energy levels coincide, and the states are brought into resonance. It is not surprising for a full integer spin system, such as **2**, to show QTM. However, according to the Kramers' spin-parity theorem,[15] QTM should not be observed in half-integer spin systems (as **1**), because the theorem dictates that no matter how asymmetric the crystal field, an ion that has an odd number of electrons has to have a ground state that is at least doubly degenerate. It is nevertheless reasonable to rationalize that QTM is occurring between entangled states of electronic and nuclear spins, similar to what was shown by Ishikawa and co-workers in other lanthanide SMMs.[7] In addition, dipolar coupling and small exchange interactions between molecules can induce tunneling.[16]

In order to bypass QTM, AC susceptibility measurements were carried out under a small optimal DC field (1000 Oe), as this shifts the χ'' maxima of the $\chi'' = f(T)$ curves to higher temperatures. For **1** and **2**, both the in-phase (χ') and the out-of-phase (χ'') components of the AC magnetic susceptibility show frequency dependence below 10 K (Figures S12 and S15). However, only complex **1** showed maxima in the temperature dependence on χ' and χ'' at the aforementioned DC field strength (Figures 6 and S14). A maximum at 9.5 K is observed for a frequency of 1000 Hz. These results correlate with other lanthanide systems, for which only the Kramers systems with odd numbers of 4f electrons (such as complex **1**) showed this DC field induced AC magnetization lag, while the non-Kramers systems (such as complex **2**) did not.[17]

The relaxation time for complex **1** shows two distinct regimes, a temperature independent quantum tunneling regime at low temperatures and a temperature dependent thermally activated regime at temperatures above 5 K. The thermally activated relaxation follows the Arrhenius law $\tau = \tau_o \exp(U_{eff}/k_BT)$. By plotting the magnetization relaxation times (τ) obtained from the AC data as ln τ versus $1/T$, it is possible to extrapolate values for the energy barrier of the relaxation of the magnetization (U_{eff}/k_B = 50 K) and the pre-exponential factor (τ_o = 6.80 × 10^{-7} s; Figure 7). These parameters are comparable to those reported for other SMMs.[6d,18] For example, for a mononuclear Dy/DOTA system, U_{eff}/k_B = 60 K,[10a] while Murugesu et al. found values for the energy barrier of the relaxation of the magnetization ranging from 20 to 101 K for dinuclear helicates.[6h]

For complex **1**, semicircular Cole−Cole plots[19] were obtained at temperatures from 1.8 to 6.0 K (Figure 8). At low temperatures, it is possible to see the appearance of the beginning of a second semicircle. This suggests that at these temperatures there are two distinct relaxation mechanisms with different characteristic times. Only one part of the semicircle was fitted to a generalized Debye model (see Supporting Information for fit information). Analysis revealed that the α parameter is close to zero, 0.12 and 0.08 for T = 5 and 6 K,

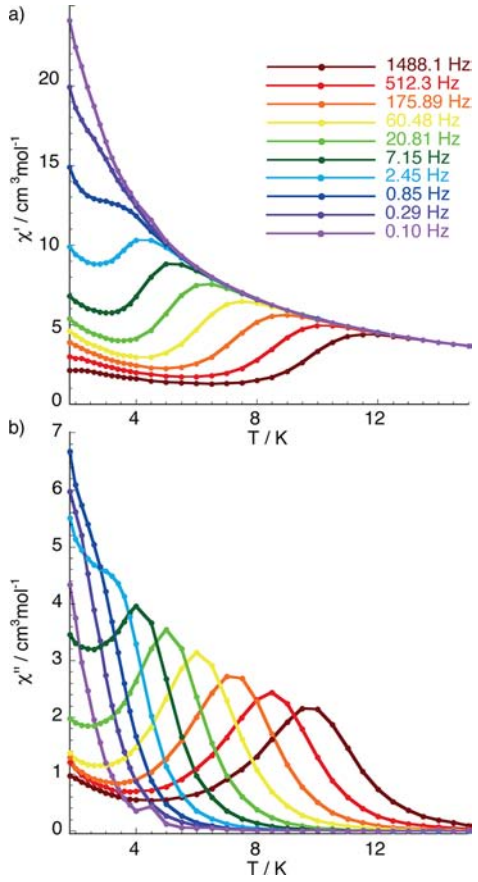

Figure 6. Data for complex **1**. Plot of χ' (a) and χ'' (b) versus temperature at different wave frequencies in the presence of a DC field (H = 1000 Oe).

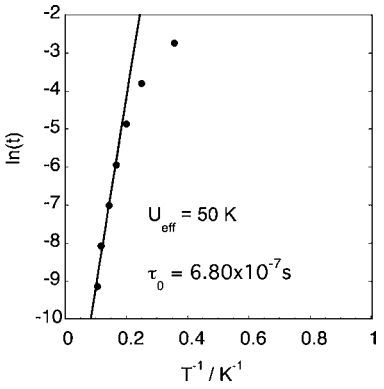

Figure 7. Data for complex **1**. Magnetization relaxation time (τ) versus 1/T; Cole−Cole plots obtained from the magnetic susceptibility data.

respectively, indicating one single relaxation time. While, in the tunneling regime, α varies between 0.21 and 0.36, which is consistent with previously reported values and is suggesting that in the tunneling regime the system is more sensitive to strain.[10b]

In order to further investigate the SMM behavior of complexes **1** and **2** and to gain insight into their low temperature behavior, single crystal magnetization measurements were performed using a micro-SQUID[14] instrument at temperatures in the range of 0.03 to 5 K. The field was aligned parallel to the easy axis of magnetization by the transverse field method.[20] Hysteresis loops were observed for both complexes.

dx.doi.org/10.1021/ic400098c | Inorg. Chem. 2013, 52, 5194−5200

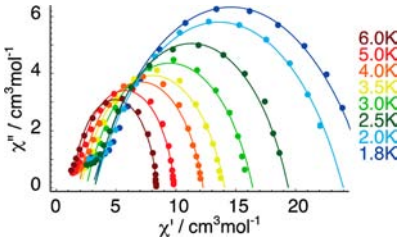

Figure 8. Data for complex **1**. Cole−Cole plots obtained from the magnetic susceptibility data. The solid black lines represent the fit obtained with a generalized Debye model with α = 0.36, 0.35, 0.29, 0.28, 0.26, 0.21, 0.12, and 0.08 sorted by increasing temperatures.

Figure 9 shows magnetization versus field measurements for **1** at a fixed temperature (0.03 K) and at varying sweep rates. The

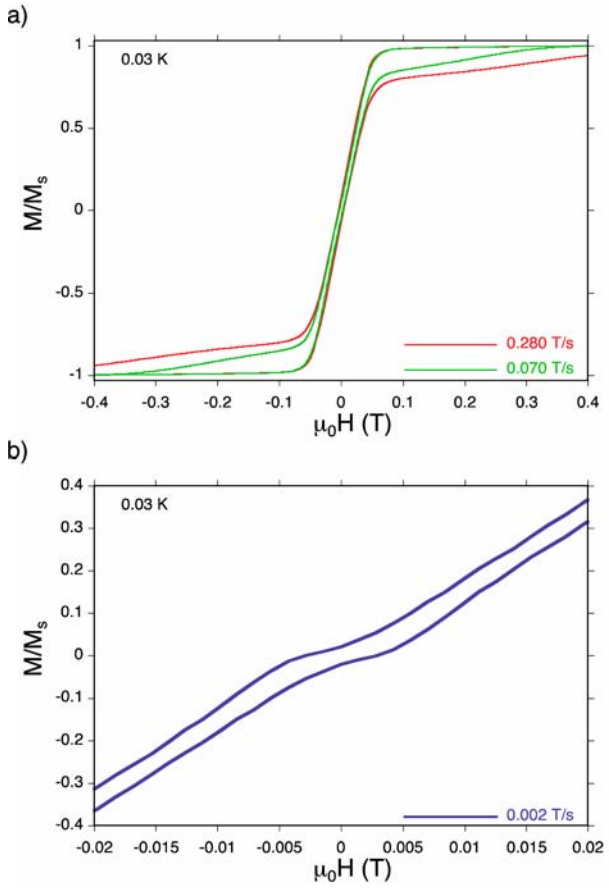

Figure 9. Hysteresis loops for **1**. (a) Full sweep at the indicated sweep rates and temperature; (b) expansion of a.

hysteresis loops have step-like features, which are indicative of QTM. Each step represents a level crossing where tunneling may occur. The system shows a strong sweep rate dependence. Generally, the coercivity of the hysteresis loops increases with decreasing temperature and increasing sweep rate (Figure S20). However, for complex **1**, the coercive field increases with increasing temperature (between 0.03 and 0.5 K), which is the opposite of what is reported for traditional SMMs. Nonetheless, this behavior is typical for SMMs with a strong tunneling rate at H = 0. Indeed, at very low temperatures most of the molecules tunnel when sweeping the field over the zero field level crossing. At high temperatures, thermal excitation reduces the net tunnel rate, and hysteresis is observed. Although hysteresis loops were observed for complex **2**, no step-like features were seen. We reasoned that magnetic dipolar interactions between adjacent molecules broadened the signals out. Therefore, no features are observed, especially the step at $\mu_0 H$ = 0 (Figure S21).

CONCLUSIONS

In conclusion, we have employed the synthetic strategy of subcomponent self-assembly in the construction of a new family of stable lanthanide-containing complexes. To the best of our knowledge this is the first example of lanthanide ions as templates in conjunction with flexible building blocks. Of this series, complexes **1** and **2** show SMM behavior. It was possible to observe step-like features in the hysteresis loops of **1** indicating QTM. Due to QTM effects, only complex **1** in the presence of a small applied DC field showed maxima in the temperature dependence of χ' and χ''. It was possible to extrapolate values for the energy barrier of the relaxation of the magnetization of U_{eff}/k_B = 50 K. Owing to the simplicity of this system, **1** can be viewed as a model upon which other self-assembled SMM molecules may be built. Current endeavors are focused on small modifications of the building blocks in order to gain a better understanding of the parameters and rules that govern SMM construction. We believe that gaining control over the self-assembly of lanthanide-containing SMM molecules is the way forward to understanding their magnetic behavior and to constructing functional materials with a higher energy barrier of the magnetization.

ASSOCIATED CONTENT

Supporting Information

Detailed magnetic studies, Cole−Cole plot fits, CIF files, IR data. This material is available free of charge via the Internet at http://pubs.acs.org.

AUTHOR INFORMATION

Corresponding Author

*E-mail: victoria.campbell@u-psud.fr.

Notes

The authors declare no competing financial interest.

ACKNOWLEDGMENTS

This work is partially financed by ANR-project MolNanoSpin No. ANR-08-NANO-002 and ERC Advanced Grant MolNanoSpin No. 226558.

REFERENCES

(1) (a) Lehn, J.-M. *Chem. Soc. Rev.* **2007**, *36*, 151. (b) Chichak, K. S.; Cantrill, S. J.; Pease, A. R.; Chiu, S.-H.; Cave, G. W. V.; Atwood, J. L.; Stoddart, J. F. *Science* **2004**, *304*, 1308. (c) Whitesides, G. M.; Mathias, J. P.; Seto, C. T. *Science* **1991**, *254*, 1312. (d) Rinehart, J. D.; Fang, M.; Evans, W. J.; Long, J. R. *Nat. Chem.* **2011**, *3*, 538.

(2) (a) Nitschke, J. R. *Acc. Chem. Res.* **2007**, *40*, 103. (b) Campbell, V. E.; de Hatten, X.; Delsuc, N.; Kauffmann, B.; Huc, I.; Nitschke, J. R. *Nat. Chem.* **2010**, *2*, 684. (c) Mal, P.; Breiner, B.; Rissanen, K.; Nitschke, J. R. *Science* **2009**, *324*, 1697. (d) Belowich, M. E.; Stoddart, J. F. *Chem. Soc. Rev.* **2012**, *41*, 2003.

(3) Thompson, M. C.; Busch, D. H. *J. Am. Chem. Soc.* **1962**, *84*, 1762.

(4) (a) Bünzli, J.-C. G. *Chem. Rev.* **2010**, *110*, 2729. (b) Eliseeva, S. V.; Bünzli, J.-C. G. *New. J. Chem.* **2011**, *35*, 1165. (c) Bünzli, J.-C. G.; Piguet, C. *Chem. Soc. Rev.* **2005**, *34*, 1048.

(5) (a) Bunzli, J. C. G.; Piguet, C. *Chem. Rev.* **2002**, *102*, 1897. (b) Bottrill, M.; Kwok, L.; Long, N. J. *Chem. Soc. Rev.* **2006**, *35*, 557.
(6) (a) Ishikawa, N.; Sugita, M.; Ishikawa, T.; Koshihara, S.-y.; Kaizu, Y. *J. Am. Chem. Soc.* **2003**, *125*, 8694. (b) Mannini, M.; Pineider, F.; Danieli, C.; Totti, F.; Sorace, L.; Sainctavit, P.; Arrio, M. A.; Otero, E.; Joly, L.; Cezar, J. C.; Cornia, A.; Sessoli, R. *Nature* **2010**, *468*, 417. (c) Blagg, R. J.; Muryn, C. A.; McInnes, E. J. L.; Tuna, F.; Winpenny, R. E. P. *Angew. Chem., Int. Ed.* **2011**, *50*, 6530. (d) Long, J.; Habib, F.; Lin, P.-H.; Korobkov, I.; Enright, G.; Ungur, L.; Wernsdorfer, W.; Chibotaru, L. F.; Murugesu, M. *J. Am. Chem. Soc.* **2011**, *133*, 5319. (e) Rinehart, J. D.; Long, J. R. *Chem. Sci.* **2011**, *2*, 2078. (f) Wang, X.-Y.; Avendaño, C.; Dunbar, K. R. *Chem. Soc. Rev.* **2011**, *40*, 3213. (g) Zaleski, C. M.; Tricard, S.; Depperman, E. C.; Wernsdorfer, W.; Mallah, T.; Kirk, M. L.; Pecoraro, V. L. *Inorg. Chem.* **2011**, *50*, 11348. (h) Habib, F.; Long, J.; Lin, P.-H.; Korobkov, I.; Ungur, L.; Wernsdorfer, W.; Chibotaru, L. F.; Murugesu, M. *Chem. Sci.* **2012**, *3*, 2158. (i) Lin, P.-H.; Burchell, T. J.; Clérac, R.; Murugesu, M. *Angew. Chem., Int. Ed.* **2008**, *47*, 8848.
(7) Ishikawa, N.; Sugita, M.; Wernsdorfer, W. *Angew. Chem., Int. Ed.* **2005**, *44*, 2931.
(8) Urdampilleta, M.; Klyatskaya, S.; Cleuziou, J.-P.; Ruben, M.; Wernsdorfer, W. *Nat. Mater.* **2011**, *10*, 502.
(9) AlDamen, M. A.; Clemente-Juan, J. M.; Coronado, E.; Martí-Gastaldo, C.; Gaita-Ariño, A. *J. Am. Chem. Soc.* **2008**, *130*, 8874.
(10) (a) Cucinotta, G.; Perfetti, M.; Luzon, J.; Etienne, M.; Car, P.-E.; Caneschi, A.; Calvez, G.; Bernot, K.; Sessoli, R. *Angew. Chem., Int. Ed.* **2012**, *51*, 1606. (b) Car, P.-E.; Perfetti, M.; Mannini, M.; Favre, A.; Caneschi, A.; Sessoli, R. *Chem. Commun.* **2011**, *47*, 3751. (c) Jiang, S.-D.; Wang, B.-W.; Su, G.; Wang, Z.-M.; Gao, S. *Angew. Chem., Int. Ed.* **2010**, *49*, 7448.
(11) Sheldrick, G. M. *SHELXS-97*; University of Göttingen, Göttingen, Germany, 1997.
(12) Sheldrick, G. M. *SHELXL-97*; University of Göttingen: Göttingen, Germany, 1997.
(13) Farrugia, L. J. *J. Appl. Crystallogr.* **1999**, 837.
(14) Wernsdorfer, W. *Supercond. Sci. Technol.* **2009**, *22*, 064013.
(15) Kramers, H. A. *Proc. R. Acad. Sci. Amsterdam* **1930**, *33*, 959.
(16) Wernsdorfer, W.; Bhaduri, S.; Boskovic, C.; Christou, G.; Hendrickson, D. *Phys. Rev. B* **2002**, *65*, 180403.
(17) Sugita, M.; Ishikawa, N.; Ishikawa, T.; Koshihara, S.-y.; Kaizu, Y. *Inorg. Chem.* **2006**, *45*, 1299.
(18) (a) Aubin, S. M. J.; Sun, Z.; Pardi, L.; Krzystek, J.; Folting, K.; Brunel, L.-C.; Rheingold, A. L.; Christou, G.; Hendrickson, D. N. *Inorg. Chem.* **1999**, *38*, 5329. (b) Layfield, R. A.; McDouall, J. J. W.; Sulway, S. A.; Tuna, F.; Collison, D.; Winpenny, R. E. P. *Chem.—Eur. J.* **2010**, *16*, 4442. (c) Bhunia, A.; Gamer, M. T.; Ungur, L.; Chibotaru, L. F.; Powell, A. K.; Lan, Y.; Roesky, P. W.; Menges, F.; Riehn, C.; Niedner-Schatteburg, G. *Inorg. Chem.* **2012**, *51*, 120420091619009.
(19) (a) Cole, K. S.; Cole, R. H. *J. Chem. Phys.* **1941**, *9*, 341. (b) Miyasaka, H.; Clérac, R.; Mizushima, K.; Sugiura, K.-i.; Yamashita, M.; Wernsdorfer, W.; Coulon, C. *Inorg. Chem.* **2003**, *42*, 8203.
(20) Ishikawa, N. *J. Phys. Chem. A* **2003**, *107*, 5831.